

Self-Tuning Position Control for the Linear Long-Stroke, Compound Switched Reluctance Conveyance Machine

J. F. Pan¹, Weiyu Wang¹, Eric Cheung², Norbert Cheung², Xiaoyu Wu¹, and Bo Zhang¹#

¹ Laboratory of Space Collaborative Manipulation Technology, Department of Automation Science, Shenzhen University, Shenzhen, China

² Department of Electrical Engineering, The Hong Kong Polytechnic University, Hunghom, Kowloon, Hong Kong, China

Corresponding Author / E-mail: zhangbo@szu.edu.cn, TEL: +86-755-26535382

ORCID: 0000-0003-1998-2377

KEYWORDS: Compound motion, LSRM, Self-tuning control

This paper proposes a long-stroke linear switched reluctance machine (LSRM) with a primary and a secondary translator for industrial conveyance applications. The secondary one can translate according to the primary one so that linear compound motions can be achieved. Considering the fact that either one translator imposes a time-variant, nonlinear disturbance onto the other, the self-tuning position controllers are implemented for the proposed linear compound machine and experimental results demonstrate that the absolute steady-state error values can fall into 0.03 mm and 0.05 mm for the secondary and primary translator, respectively. A composite absolute precision of less than 0.6 mm can be achieved under the proposed control strategy.

Manuscript received: February 8, 2017 / Revised: June 13, 2017 / Accepted: December 11, 2017

NOMENCLATURE

$h = 1$ and 2 , stands for the primary and the secondary translator, respectively

j = phase windings with $j = AA'$, BB' and CC'

U_{hj} = supply phase voltage

i_{hj} = phase current

R_{hj} = phase resistance

φ_{hj} = phase flux linkage

x_h = displacement

L_{hj} = phase inductance

f_1, f_{11} and f_2, f_{12} = generated electromechanical force and load force for the primary and secondary translator, respectively

M and m = the mass of the primary and secondary translator

Q_h = friction coefficient of the two translators

f_{hj} = force command

i_{hj}^* = current command

e_h = disturbance

a_{h1}, a_{h2}, b_{h0} and b_{h1} = system parameters

A_h and B_h = system denominator and numerator polynomials, respectively

G_h = gain matrix

P_h = covariance matrix

ρ_h = the forgetting factor

θ_h = identification matrix

δ = a small positive number

A_{hm}, B_{hm} = desired pole and zero polynomial

A_{h0} = observer polynomial

$u_h(z^{-1})$ = control input

R_h, T_h and S_h = polynomials of self-tuning controller

1. Introduction

In modern manufacturing and assembly industry, electrical or mechanical components or parts rely on conveyance systems to transport them to arrive at proper positions for further processing. For linear transportations, rotary machines with synchronous belts are sometimes involved to realize conveyance systems. Due to wear and aging of the belts and other mechanical parts, the precision of the entire conveyance system is often hard to be guaranteed.¹ The traditional method of rotary machines and belts can be replaced by direct-drive, linear machines, which have the advantages of fast response, high-precision and speed.² For linear conveyance systems nowadays, the speed of the moving part

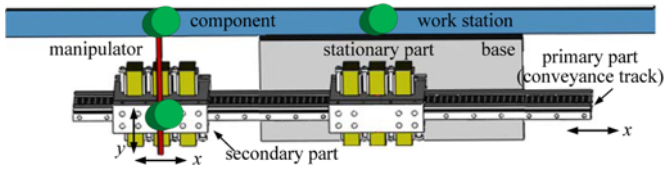


Fig. 1 Concept of the direct-drive, compound linear conveyance system

should often be kept at specified values for sequenced processing of the components or parts.⁴ Two or more transportation tasks can rarely be handled at the same time.

If any secondary moving part (or translator) can be embedded onto the linear conveyance system and the moving part makes relative motions according to the primary conveyance one at the same time, then the efficiency of the entire component transportation task can be increased. As shown in Fig. 1 the concept of a direct-drive, compound linear conveyance system, the stationary part propels the conveyance track (primary part) along the x axis, and the manipulator is responsible to transport the components to a certain work station along the y direction. The secondary part is embedded onto the conveyance track and the secondary translator is capable of translation along the conveyance track. It can be seen that the secondary part can work simultaneously as the conveyance track translates. Thus, the processing time can be reduced with increased component conveyance efficiency. Meanwhile, the entire positioning precision of the linear conveyance system can be improved, if both the conveyance track and the secondary part can work coordinately.

For direct-drive translational machines, a linear induction motor is more suitable for long-range transportation purposes.⁵ However, it is difficult to realize a compound machine structure for composite motions due to the induction machine methodology.⁶ A linear permanent magnet (PM) machine is more suitable for high-speed, high-precision applications, nevertheless, the complicated winding structure prevents the utilization for long-range conveyance purposes.⁷⁻⁹ The arrangement of PM blocks further increases system cost and complexity, especially for long-stroke operations.⁷ In addition, temperature variations inevitably result in performance deterioration or even malfunction of the machines.⁸ A linear switched reluctance motor (LSRM) has the merits of simple construction and easy implementation. Owing to a robust and stable mechanical structure, it is particularly suitable for the operation under long-range applications.⁹⁻¹²

For the composite operation of an integrated LSRM, either the primary or the secondary part acts as an external, time-variant, load disturbance onto each other. Since the position control performance of LSRMs is highly dependent on both position and current,^{13,14} the primary or the secondary part inevitably imposes a dynamic temporal-spatial influence onto each other. Therefore, it is necessary to identify such influence qualitatively in real time and correct such disturbance accordingly. It is very difficult for a traditional proportional-integral-differential (PID) controller to cope with such disturbances since its design is mainly based on the static model of a system.¹⁵ To achieve a high-precision position control performance, the dynamic models for the primary and secondary parts should be established for uniform

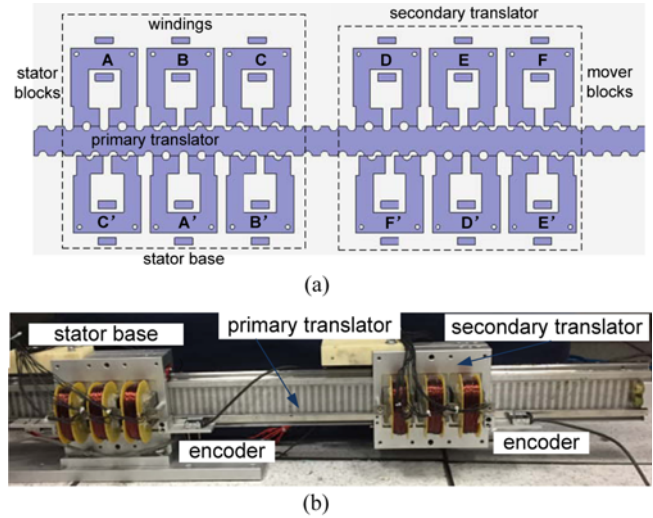


Fig. 2 The structure (a) and picture (b) of the LSRM

operations.^{16,17} According to current literature, a nonlinear proportional differential (PD) controller is introduced for the LSRM to achieve a better dynamic response; in Ref. 17, a passivity-based control algorithm is proposed for a position tracking system of the LSRM to overcome the inherent nonlinear characteristics and render system robustness against uncertainties. However, the above nonlinear algorithms fail to identify and correct the influence of external disturbances in real time. Therefore, online parameter identification is a good choice to characterize the dynamic models for both parts.¹⁸ In addition, a self-tuning position controller is capable of adjusting control parameters based on the dynamic behaviors to achieve a designated position control performance, according to the desired poles.¹⁵

In this paper, a long LSRM with primary and secondary translators is first introduced. Then, online system identification scheme is introduced to calculate the model parameters in real time, based on the recursive least square (RLS) method. Next, the self-tuning position controllers based on the pole-placement methodology are constructed to realize a uniform position control performance for both translators. The contribution of this paper is two folded. First, a compound LSRM for industrial conveyance applications is proposed and constructed. This machine has the characteristics of long stroke and the capability of composite linear motions. Second, by applying the self-tuning position control strategy, both independent position control and composite control can be realized to achieve a better, uniform performance, compared to the PID controllers.

2. Structure and Principle of the LSRM

According to the switched reluctance principle, the compound linear machine can either conform to a single-sided or double-sided topology. Fig. 2(a) demonstrates the schematic view of the compound machine. It mainly consists of a stator base with stator/mover blocks. The proposed machine utilizes an asymmetric structure. Instead of perfect mirror along the axis of the primary stator, either the stator phases or the mover phases apply an asymmetric scheme to improve a higher force-to-

Table 1 Major specifications

Variable	Parameters	Unit
Mass of primary/secondary translator (M/m)	15.2/5	kg
Rated power	250	W
Pole width	6	mm
Pole pitch	12	mm
Phase resistance	3	ohm
Air gap length	0.3	mm
Stack length	200	mm
Number of phases	3	-
Number of teeth primary/secondary translator (stator)	83/24	-
Stroke of primary/secondary translator	3.4/1.4	m

volume ratio and efficiency.^{3,19} Fig. 2(b) is the picture of the machine prototype.

The stator base and the secondary translator have the same dimensions and ratings. The windings are three phased and each phase is serially connected, marked as AA', BB', CC' for the stator or the secondary translator. When the windings of the stator base are properly excited, the primary translator translates according to the stator base; if the windings of the secondary translator are activated, it moves with respect to the primary translator, which is two meters in total length. Therefore, a composite movement can be achieved from the primary and the secondary translators. Table 1 lists the major specifications of the proposed LSRM.

The voltage balancing equation can be characterized as the following,²¹

$$U_{hj} = R_{hj}i_{hj} + \frac{\partial \varphi_{hj}(x_h, i_{hj})}{\partial x_h} \frac{dx_h}{dt} + \frac{\partial \varphi_{hj}(x_h, i_{hj})}{\partial i_{hj}} \frac{di_{hj}}{dt} \quad (1)$$

Under unsaturated regions, the propulsion force of any phase for any translator can be formulated as,⁸

$$f_{hj} = \frac{1}{2} \cdot \frac{dL_{hj}(x_h, i_{hj})}{dx_h} i_{hj}^2 \quad (2)$$

The kinetic equations for the primary and secondary translator can be represented as Eqs. (3) and (4), respectively.

$$f_1 = (M+m) \times \frac{d^2x_1}{dt^2} + \sum_{h=1}^2 Q_h \frac{dx_h}{dt} + f_{l_1} \quad (3)$$

$$f_2 = m \times \frac{d^2x_2}{dt^2} + \sum_{h=1}^2 Q_h \frac{dx_h}{dt} + f_{l_2} \quad (4)$$

It is clear from the above two equations that the generated force from either one translator affects the behavior of the other.

3. Compound Position Control System

The compound position control diagram is illustrated as shown in Fig. 3. For any translator, the multi-phase excitation scheme in the force control loop decides which phase(s) should be excited, based on current position and force command f_{hj} . Then current command i_{hj}^* of each phase can be derived, according to Table 2.¹⁵ Last, the current loop of each phase generates the actual current output i_{hj} for each phase according to the current command i_{hj}^* . When the switch is in the "off

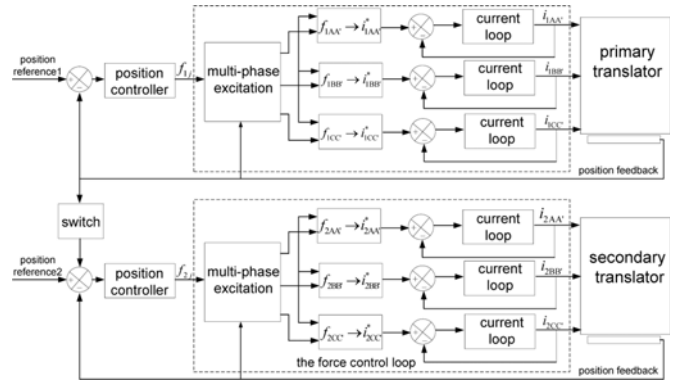


Fig. 3 Compound control diagram

Table 2 Multi-phase excitation scheme

Range (mm)	positive force command	negative force command
0-2	$f_{hBB'} = f_{hj}$	$f_{hCC'} = 0.5(2-x_h)f_{hj}$ $f_{hAA'} = 0.5x_h f_{hj}$
2-4	$f_{hBB'} = 0.5(4-x_h)f_{hj}$ $f_{hCC'} = 0.5(x_h-2)f_{hj}$	$f_{hAA'} = f_{hj}$
4-6	$f_{hCC'} = f_{hj}$	$f_{hAA'} = 0.5(6-x_h)f_{hj}$ $f_{hBB'} = 0.5(x_h-4)f_{hj}$
6-8	$f_{hCC'} = 0.5(8-x_h)f_{hj}$ $f_{hAA'} = 0.5(x_h-6)f_{hj}$	$f_{hBB'} = f_{hj}$
8-10	$f_{hAA'} = f_{hj}$	$f_{hBB'} = 0.5(10-x_h)f_{hj}$ $f_{hCC'} = 0.5(x_h-8)f_{hj}$
10-12	$f_{hAA'} = 0.5(12-x_h)f_{hj}$ $f_{hBB'} = 0.5(x_h-10)f_{hj}$	$f_{hCC'} = f_{hj}$

state, each translator receives its own position reference signal. This means that each translator can be controlled independently. The two systems can then be decoupled through their own position feedback signal, and therefore, the primary translator performs linear movement relative to the ground, while the secondary translator performs linear movement relative to the primary translator. If the switch is in the "on state, the real time position feedback signal from the primary translator is imposed and serves as another reference position signal to the secondary translator. Thus, the movement of the secondary translator can be superimposed. Therefore, a composite linear movement can be achieved through the secondary translator according to ground.

From Eq. (3) and (4), the position control system for the primary or secondary translator can be represented as second-order systems with the force command as the system input and position as the system output, respectively. The second-order system can be rewritten in the discrete-time form considering disturbance e_h as,

$$A_h(z^{-1})x_h(z^{-1}) = B_h(z^{-1})f_h(z^{-1}) + e_h(z^{-1}) \quad (5)$$

$$\begin{cases} A_h(z^{-1}) = 1 + a_{h1}z^{-1} + a_{h2}z^{-2} \\ B_h(z^{-1}) = b_{h0}z^{-1} + b_{h1}z^{-2} \end{cases} \quad (6)$$

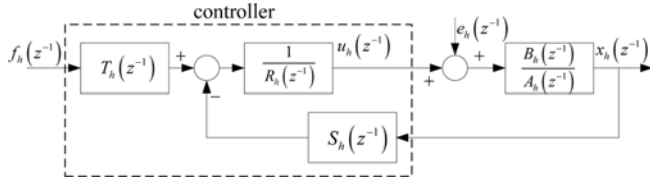


Fig. 4 Position controller

3.1 Recursive least square algorithm with forgetting factor

Since the recursive least square algorithm is suitable for time-variant, nonlinear systems, it is applied for the identification of the above system parameters. Eq. (5) is further transformed into the least square form as,

$$x_h(z^{-1}) = \varphi_h^T(z^{-2})\theta_h(z^{-2}) + e_h(z^{-1}) \quad (7)$$

where, $\varphi_h(z^{-2}) = [-x_h(z^{-2}) - x_h(z^{-3})f_h(z^{-1})f_h(z^{-2})]^T$, $\theta_h(z^{-2}) = [a_{h1}a_{h2}b_{h0}b_{h1}]^T$ and $e_h(z^{-1})$ is the residual. The parameters can be calculated by the following as,²²

$$\theta_h(z^{-1}) = \theta_h(z^{-2}) + G_h(z^{-1})[x_h(z^{-1}) - \varphi_h^T(z^{-1})\theta_h(z^{-2})] \quad (8)$$

$$G_h(z^{-1}) = P_h(z^{-2})\varphi_h(z^{-1})[\rho_h + \varphi_h^T(z^{-1})P_h(z^{-2})\varphi_h(z^{-1})]^{-1} \quad (9)$$

$$P_h(z^{-1}) = \frac{1}{\rho_h}[I - G_h(z^{-1})\varphi_h^T(z^{-1})]P_h(z^{-2}) \quad (10)$$

The forgetting factor should be chosen at the interval (0.9 1), to avoid identification data saturation.²² The smaller the value the faster the forgetting is. For initial values, $P_h(0) = rI_{4 \times 4}$ with r as a constant value of 100,000 and $I_{4 \times 4}$ is a four-dimension unit matrix. If the relative error from the last and present step is comparatively small, it is regarded that the present estimated value is correct. Then the criterion to terminate the recursive calculation can be set as,

$$\left| \frac{\widehat{\theta}(z^{-2}) - \widehat{\theta}(z^{-1})}{\widehat{\theta}(z^{-1})} \right| < \delta \quad (11)$$

3.2 Self-tuning position control based on pole-assignment

The self-tuning control algorithm adjusts the control parameters based on the pole-placement scheme, according to the current identified parameters.²³ Therefore, the entire control system can be operated in an optimized condition according to the desired system predefined poles.²³ The control structure of the self-tuning position controller is shown in Fig. 4.

The controller algorithm can thus be depicted as,²³

$$R_h(z^{-1})u_h(z^{-1}) = T_h(z^{-1})f_h(z^{-1}) - S_h(z^{-1})x_h(z^{-1}) \quad (12)$$

The polynomials R_h , T_h and S_h from the controllers satisfy the causality conditions $\deg S_h \leq \deg R_h$ and $\deg T_h \leq \deg R_h$. Then we have,

$$\begin{cases} x_h(z^{-1}) = \frac{B_h T_h}{A_h R_h + B_h S_h} f_h(z^{-1}) + \frac{B_h R_h}{A_h R_h + B_h S_h} e_h(z^{-1}) \\ u_h(z^{-1}) = \frac{A_h T_h}{A_h R_h + B_h S_h} f_h(z^{-1}) - \frac{B_h S_h}{A_h R_h + B_h S_h} e_h(z^{-1}) \end{cases} \quad (13)$$

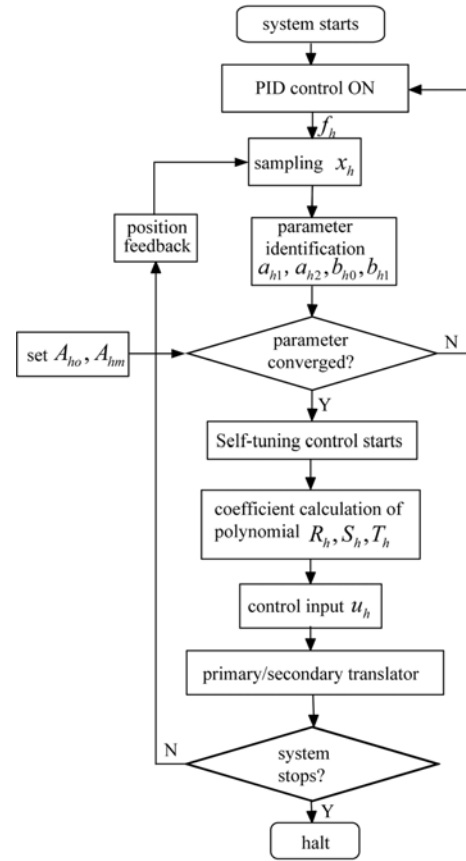


Fig. 5 Program flow of position control

$$\frac{B_h T_h}{A_h R_h + B_h S_h} = \frac{B_{hm}}{A_{hm}} \quad (14)$$

The closed loop characteristic equation can thus be described as,

$$A_h R_h + B_h S_h = A_{hc} = A_{ho} A_{hm} \quad (15)$$

Causality conditions are denoted as follows,

$$\begin{cases} \deg A_{hc} \geq 2 \deg A_h - 1 \\ \deg A_{hm} - \deg B_{hm} \geq \deg A_h - \deg B_h \end{cases} \quad (16)$$

where polynomials A_{hm} and B_{hm} contain the desired closed loop poles and zeros, respectively. For second-order systems, we have,²³

$$\begin{cases} A_{h0}(z^{-1}) = 1 + a_{h0} \cdot z^{-1} \\ A_{hm}(z^{-1}) = 1 + a_{hm1} \cdot z^{-1} + a_{hm2} \cdot z^{-2} \end{cases} \quad (17)$$

$$\begin{cases} R = 1 + r_1 z^{-1} + r_2 z^{-2} \\ S = s_0 + s_1 z^{-1} \\ T = t_0 + t_1 z^{-1} \end{cases} \quad (18)$$

The control program flow chart for each translator can be depicted as shown in Fig. 5. Since persistent excitation is required to make the estimated parameters to converge to their real values, each position control system is first controlled by the PID controller. After system

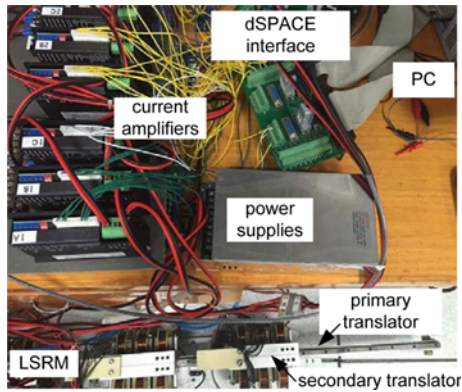


Fig. 6 Experimental setup

Table 3 Control parameter regulation values

Control parameter	Value	Control parameter	Value
P_1	4.173	P_2	3.985
D_1	0.031	D_2	0.029
I_1	0.01	I_2	0.01
a_{1m1}	-1.942	a_{2m1}	-1.937
a_{1m2}	0.944	a_{2m2}	0.938
a_{10}	-0.896	a_{20}	-0.903
ρ_1	0.997	ρ_2	0.995

note: the desired poles for the primary and secondary translators are $0.967 \pm 0.094i$ and $0.9685 \pm 0.0028i$, respectively

parameters enter the steady-state, control decision is switched to the self-tuning controller. Detailed coefficients calculation r_1, r_2, s_0, s_1, t_0 and t_1 of polynomials R_h, S_h and T_h can be found in Refs. 19, 22.

4. Experimental Results

The entire experiment is conducted on the dSPACE DS1104 control platform, and the developed program can be directly downloaded to the digital signal processor of the control board. Commercial current amplifiers are adopted to acquire the desired current for each phase. Two identical linear magnetic encoders with the resolution of $10 \mu\text{m}$ are adopted. The sampling frequency for the position control loop is 1 kHz. Fig. 6 shows the overall experimental setup.

To simulate the positioning of the machine for component transportations, the nominal state for parameter regulations is set as 40 mm amplitude with the frequency of 0.5 Hz square reference signal. The dynamic response can be found in Fig. 7, if the two translators are separately activated. The PID parameters for each translator are regulated individually, such that a minimum steady-state error values can be achieved under the nominal condition. The PID parameters are listed in Table 3. The coefficients of the desired pole polynomials are selected to theoretically acquire a zero steady-state error according to the reference signal.²³

As shown from Fig. 7(a), the dynamic performance from the two translators is almost the same. However, the dynamic responses from the positive transitions to the negative transitions are not uniform for either translator. There exhibits dominant overshoots from the negative

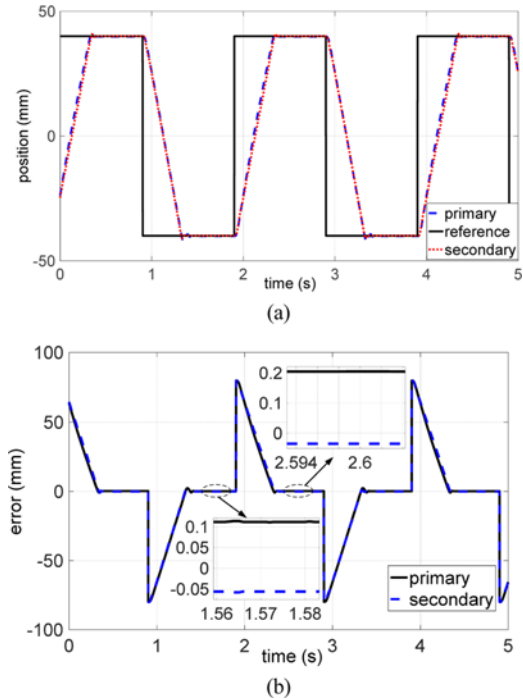


Fig. 7 Experimental results of individual operation from PID (a) response (b) error

transitions. This is due to the different mathematic models from the positive and negative transitions. The reason may originate from the asymmetric behaviors such as friction coefficients or difference of manufacture, etc.²⁰ From Fig. 7(b), the steady-state error values for the primary translator from the positive and negative transitions fall into 0.2 mm and 0.1 mm, respectively; the maximum absolute steady-state error values for the secondary translator are -0.05 mm and -0.049 mm.

Under PID regulation, the parameter identification is performed at the nominal state for each translator individually. As shown in Figs. 8(a) and (b) the identification results, all parameters reach to their stable values within 5 seconds. After all the parameters are converged, the control algorithm is switched to the self-tuning control method. From the dynamic response profiles illustrated in Figs. 8(c) and (d), the dynamic response waveforms almost overlap for the primary and secondary translator, and a symmetric steady-state error performance can be achieved for either positive or negative transitions. The steady-state error values are 0.05 mm and 0.03 mm for the primary and secondary translator, respectively.

If the “switch” in Fig. 3 is turned off and the position reference signals are identical, then a simultaneous movement can be achieved for the two translators. Though the two translators move together, each follows its own reference signal independently. Figs. 9(a) and (c) demonstrate the dynamic response profiles of the two translators under PID and self-tuning control, respectively. Under the same control parameters, the PID controllers for each translator are no longer able to remain the same control performance, since time-variant disturbances from the translators are existent. The steady state has not even dwelled during the negative transitions. For the self-tuning position controllers, however, the control performance remains the same. This is because the self-tuning controller can regulate the control parameters in time,

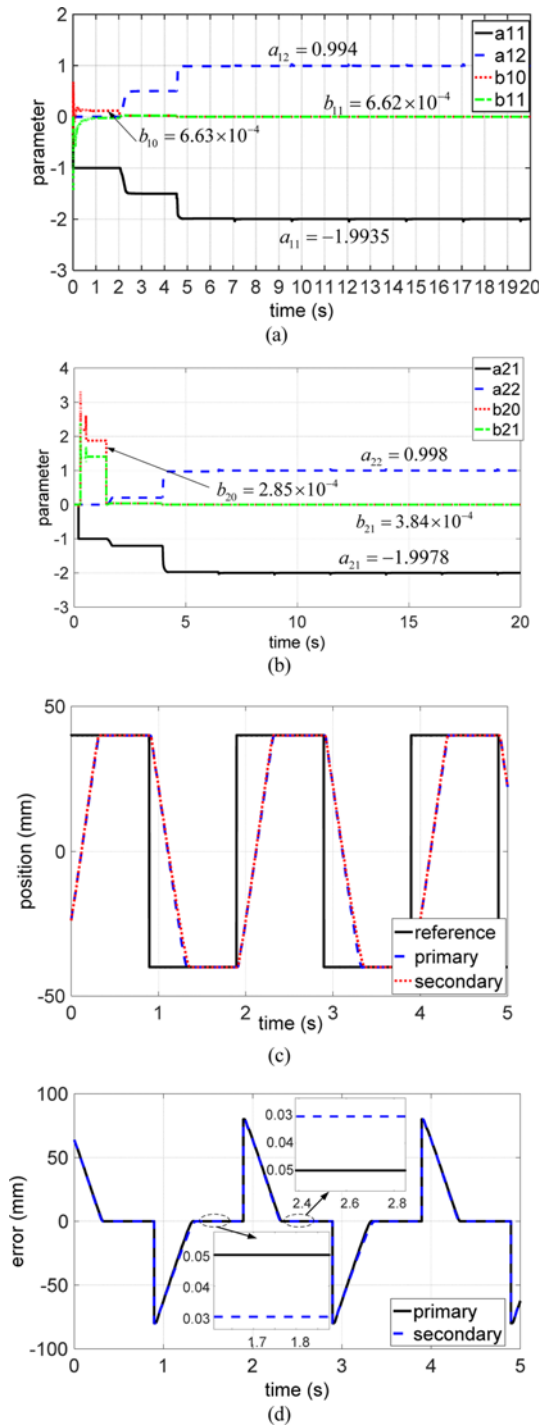


Fig. 8 Identification converging profiles (a) and (b), individual operation from self-tuning control (c) response (d) error

according to the designated desired poles. The speed profiles of the primary and the secondary translator can be illustrated in Fig. 9(b). It is clear that an accumulated speed to ground can be obtained.

If the switch is “on”, then the position feedback signal of the primary translator can serve as the part of the reference signal for the secondary translator. Thus, a compound linear movement to ground can be achieved. For example, in the conveyance industry, the primary translator is often required to perform reciprocal motions among different work stations for component conveyance. If an emergency occurs at some

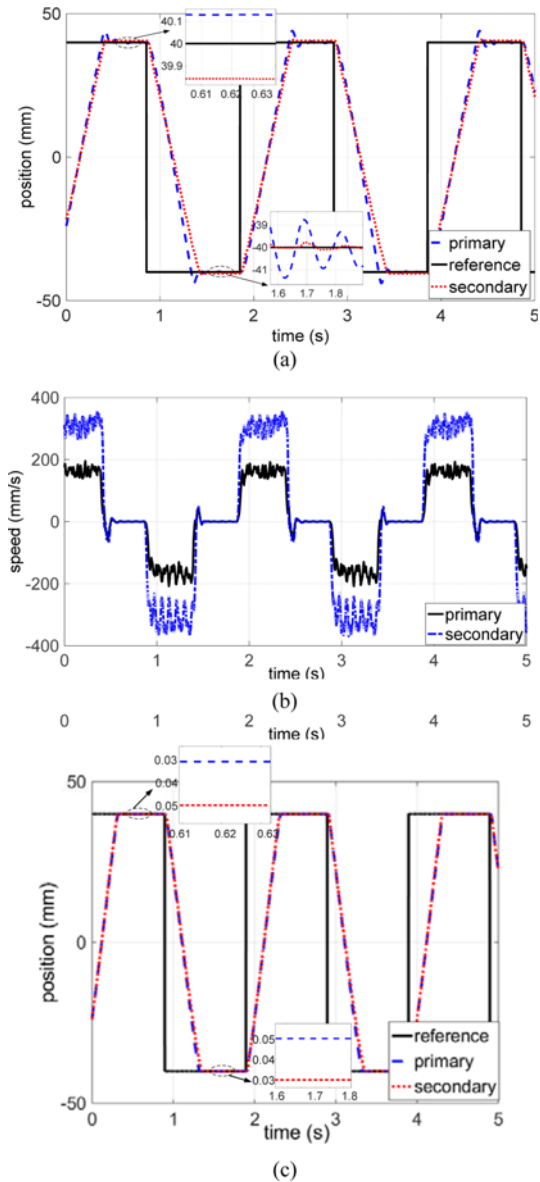


Fig. 9 Results of operation from PID (a) and (b) speed profiles (c) response under self-tuning control

work station, and at the same time, the primary translator cannot respond to such emergency, then the secondary translator can take this job for this emergency response. As shown in Fig. 10(a), the actual position signal for the primary translator is a sinusoidal waveform of amplitude ± 40 mm and 0.2 Hz. To quickly respond to the emergency, the reference position signal to ground is a perfect square waveform to ground. Then the reference signal for the secondary translator according to the primary one can thus be derived as the blue dashed lines, as shown in Fig. 10(a). According to Fig. 10(b), a compound linear motion according to ground can be realized from the secondary translator for a square waveform with amplitude of 80 mm. This compound operation successfully simulates the above situation, it can be seen that the tracking error values from the primary translator fall into 0.4 mm; while the maximum steady-state error falls into 0.2 mm for the secondary translator. Therefore, the compound precision from the secondary translator to ground does not exceed 0.6 mm.

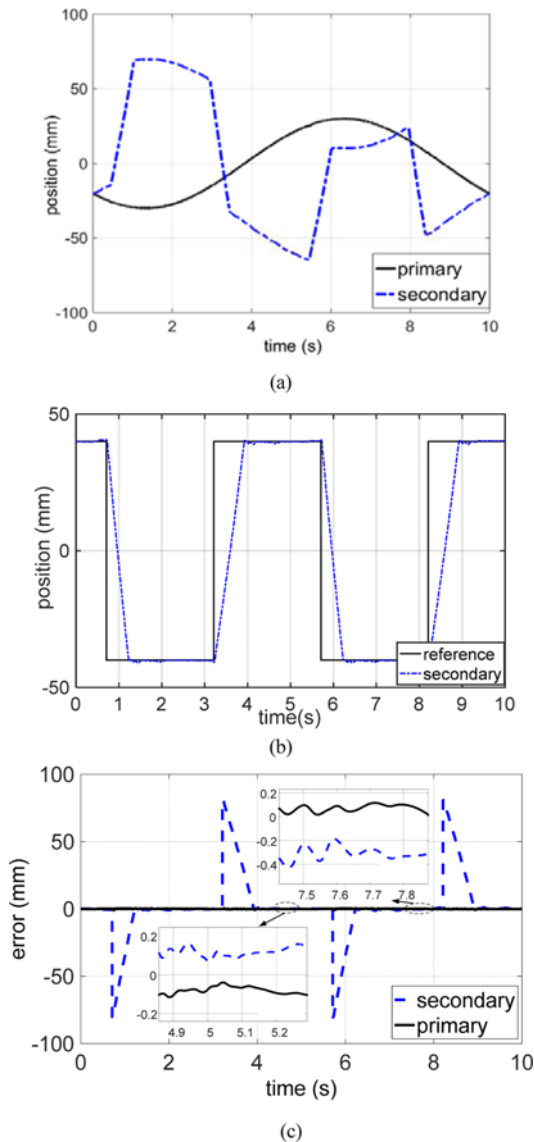


Fig. 10 Results of compound (a) response of the primary and reference signal to the secondary translator (b) response of the secondary translator and reference signal to ground (c) error profiles

5. Conclusions & Discussions

A linear compound switched reluctance machine that consists of a primary moving part and a secondary translation part is proposed in this paper. This machine is able to realize a composite linear motion from the secondary translator to ground. By the implementation of the self-tuning position control strategy, the steady-state error values can be controlled within ± 0.03 mm and ± 0.05 mm for the secondary and primary translator, respectively, under the nominal square wave reference signals. This proposed machine successfully simulates a linear conveyance system operation in a constant sinusoidal reference signal, while the secondary translator responds to emergency at the same time. To realize the composite motion to ground in a square waveform of amplitude ± 40 mm and 0.2 Hz, experimental results demonstrate that the compound precision is less than ± 0.6 mm.

From the above analysis, all control parameters are regulated under

the nominal state. In addition, since parameter identification schemes often require enough steady states from the control process,²² the control performance under the composite motion is not optimized. It is recommended that some control algorithms under reference signals with continuous variations to be included for the proposed linear machine.

ACKNOWLEDGEMENT

This work was supported by the National Natural Science Foundation of China under Grant 51477103, 51577121 and 51575360, and in part by the Guangdong Natural Science Foundation under Grant S2014A03 0313564, 2015A010106017 and 2016KZDXM007. The authors would also like to thank Shenzhen Government under code JCYJ2016030810 4825040 for support.

REFERENCES

1. Cao, R., Cheng, M., and Zhang, B., "Speed Control of Complementary and Modular Linear Flux-Switching Permanent-Magnet Motor," *IEEE Transactions on Industrial Electronics*, Vol. 62, No. 7, pp. 4056-4064, 2015.
2. Cao, R., Cheng, M., Mi, C., Hua, W., Wang, X., and Zhao, W., "Modeling of a Complementary and Modular Linear Flux-Switching Permanent Magnet Motor for Urban Rail Transit Applications," *IEEE Transactions on Energy Conversion*, Vol. 27, No. 2, pp. 489-497, 2012.
3. Pan, J. F., Zou, Y., and Cao, G., "An Asymmetric Linear Switched Reluctance Motor," *IEEE Transactions on Energy Conversion*, Vol. 28, No. 2, pp. 444-451, 2013.
4. Hellinger, R. and Mnich, P., "Linear Motor-Powered Transportation: History, Present Status, and Future Outlook," *Proceedings of the IEEE*, Vol. 97, No. 11, pp. 1892-1900, 2009.
5. Cao, R. W., Jin, Y., and Zhang, Y. Z., "Design and Analysis a New Primary HTS Linear Motor for Transportation System," *Proc. of IEEE International Conference on Applied Superconductivity and Electromagnetic Devices (ASEMD)*, pp. 218-219, 2015.
6. Thomas, J. and Hansson, A., "Speed Tracking of a Linear Induction Motor-Enumerative Nonlinear Model Predictive Control," *IEEE Transactions on Control Systems Technology*, Vol. 21, No. 5, pp. 1956-1962, 2013.
7. Zhang, Z., Cheung, N. C., Cheng, K. W. E., Xue, X. D., and Lin, J. K., "Longitudinal and Transversal End-Effects Analysis of Linear Switched Reluctance Motor," *IEEE Transactions on Magnetics*, Vol. 47, No. 10, pp. 3979-3982, 2011.
8. Baoming, G., de Almeida, A. T., and Ferreira, F. J., "Design of Transverse Flux Linear Switched Reluctance Motor," *IEEE Transactions on Magnetics*, Vol. 45, No. 1, pp. 113-119, 2009.
9. Suzuki, K., Kim, Y.-J., and Dohmeki, H., "Proposal of the Section Change Method of the Stator Block of the Discontinuous Stator

- Permanent Magnet Type Linear Synchronous Motor Aimed at Long-Distance Transportation,” Proc. of 18th International Conference on Electrical Machines, pp. 1-6, 2008.
10. Pan, J. F., Zou, Y., Cheung, N., and Cao, G.-z., “On the Voltage Ripple Reduction Control of the Linear Switched Reluctance Generator for Wave Energy Utilization,” IEEE Transactions on Power Electronics, Vol. 29, No. 10, pp. 5298-5307, 2014.
 11. Masoudi, S., Feyzi, M. R., and Sharifian, M. B. B., “Force Ripple and Jerk Minimisation in Double Sided Linear Switched Reluctance Motor Used in Elevator Application,” IET Electric Power Applications, Vol. 10, No. 6, pp. 508-516, 2016.
 12. Li, W., Chen, C.-Y., Yan, L., Jiao, Z., and Chen, I.-M., “Design and Modeling of Tubular Double Excitation Windings Linear Switched Reluctance Motor,” Proc. of IEEE 10th Conference on Industrial Electronics and Applications (ICIEA), pp. 1686-1691, 2015.
 13. Ahmad, S. S., and Narayanan, G., “Linearized Modeling of Switched Reluctance Motor for Closed-Loop Current Control,” IEEE Transactions on Industry Applications, Vol. 52, No. 4, pp. 3146-3158, 2016.
 14. Zhong, R., Wang, Y. B., and Xu, Y. Z., “Position Sensorless Control of Switched Reluctance Motors Based on Improved Neural Network,” IET Electric Power Applications, Vol. 6, No. 2, pp. 111-121, 2012.
 15. Zhao, S. W., Cheung, N. C., Gan, W.-C., Yang, J. M., and Pan, J. F., “A Self-Tuning Regulator for the High-Precision Position Control of a Linear Switched Reluctance Motor,” IEEE Transactions on Industrial Electronics, Vol. 54, No. 5, pp. 2425-2434, 2007.
 16. Wang, A., Xu, W., and Liu, C.-T., “On-Line Pi Self-Tuning Based on Inertia Identification for Permanent Magnet Synchronous Motor Servo System,” Proc. of International Conference on Power Electronics and Drive Systems, pp. 1406-1410, 2009.
 17. Zhao, S., Cheung, N. C., Gan, W. C., Yang, J., and Zhong, Q., “Passivity-Based Control of Linear Switched Reluctance Motors with Robustness Consideration,” IET Electric Power Applications, Vol. 2, No. 3, pp. 164-171, 2008.
 18. Cheung, N. C., Pan, J. F., and Li, J.-Q., “Real-Time On-Line Parameter Estimation of Linear Switched Reluctance Motor,” Proc. of XIX International Conference on Electrical Machines (ICEM), pp. 1-5, 2010.
 19. Chen, H. and Wang, Q., “Electromagnetic Analysis on Two Structures of Bilateral Switched Reluctance Linear Motor,” IEEE Transactions on Applied Superconductivity, Vol. 26, No. 4, pp. 1-9, 2016.
 20. Pan, J. F., Zou, Y., and Cao, G., “Adaptive Controller for the Double-Sided Linear Switched Reluctance Motor Based on the Nonlinear Inductance Modelling,” IET Electric Power Applications, Vol. 7, No. 1, pp. 1-15, 2013.
 21. Krishnan, R., “Switched Reluctance Motor Drives: Modeling, Simulation, Analysis, Design, and Applications,” CRC Press, 2017.
 22. Ljung, L., “System Identification,” in: Signal Analysis and Prediction, Procházka A., Uhlř J., Rayner P. W. J., Kingsbury N. G. (Eds.), Springer, pp. 163-173, 1998.
 23. Åström K. J. and Wittenmark B., “Adaptive Control,” Addison-Wesley Publishing Company, 1995.